RSC Advances

PAPER

View Article Online
View Journal | View Issue

Cite this: *RSC Adv.*, 2017, **7**, 33568

Highly permeable ionic liquid 1-butyl-3-methylimidazoliumtetrafluoroborate ($BMIMBF_4$)/CuO composite membrane for CO_2 separation

Young Sung Park, Chaeyeon Ha and Sang Wook Kang *

Received 28th April 2017
Accepted 26th June 2017

DOI: 10.1039/c7ra04797e

rsc.li/rsc-advances

An ionic liquid (IL) 1-butyl-3-methylimidazoliumtetrafluoroborate ($BMIM^+BF_4^-$)/CuO composite was prepared for CO_2 transport membranes. CuO nanoparticles (NPs) were successfully generated in $BMIM^+BF_4^-$. The formation of CuO NPs was ascribed to the favorable interaction between the ions of $BMIM^+BF_4^-$ and the surface of the CuO particles. To confirm the coordination behavior of the $BMIM^+BF_4^-$/CuO membrane, TGA and FT-Raman spectroscopy were employed. The ideal CO_2/N_2 selectivity in the case of the composite material was 21.0, with a CO_2 permeance of 52.4 GPU, while the neat $BMIM^+BF_4^-$ membrane showed a selectivity of 5.0 and a CO_2 permeance of 17.0 GPU. The enhanced separation performance was attributed to (1) the synergistic effect of well-dispersed CuO nanoparticles, resulting in enhanced CO_2 solubility due to the increased surface of the oxide particle layer and (2) the abundant free ions in $BMIM^+BF_4^-$.

I. Introduction

Presently, one of the greatest challenges for researchers is finding a thermodynamically efficient process for separating and capturing CO_2.[1] It has been commonly accepted that global warming is related directly to the increased levels of CO_2.[2–4] CO_2 is mainly emitted as a result of the combustion of fossil fuels, certain chemical plant processes, and production of synthesis gas.[5] Currently, the principal CO_2 separation technologies for post-combustion capture include physical adsorption, physical or chemical absorption, cryogenic distillation, and membrane separation.[6,7] Among the various types of CO_2 separation technologies, membrane technology promises excellent separation performance while being relatively less energy- and capital intensive.[8–11] However, current commercial polymeric membranes, such as polyimide and cellulose acetate membranes, have low CO_2 selectivity and permeability, since they are based on a solution-diffusion mechanism and rely chiefly on the subtle size differences of the penetrants to accomplish separation.[12,13] To overcome the low separation performance of polymeric membranes, facilitated transport was introduced so that higher gas permeability and outstanding selectivity could be achieved.[14–16] The facilitated transport membrane has attracted attention due to the reversible reaction with a specific gas component.[17] Hence, the reaction in the membrane can generate another transport mechanism alongside the simple solution-diffusion mechanism.[18,19]

Given the above, ionic liquids (ILs) have been utilized to prepare facilitated CO_2 transport membranes.[20,21] ILs have attracted great attention because of their highly tunable properties such as low flammability, high chemical and thermal stability, and extremely low volatility.[22] Moreover, ILs based on imidazolium cations present outstanding CO_2 separation performance since the amine group in the imidazolium ring acts a CO_2 carrier in CO_2/CH_4 and CO_2/N_2 separation.[23] For example, CO_2 separation performance utilizing 1-butyl-3-methylimidazolium tetrafluoroborate ($BMIM^+BF_4^-$) showed that CO_2/N_2 and CO_2/CH_4 ideal selectivity were 5 and 4.8, respectively.[24] Surprisingly, the CO_2 permeance was 17 GPU.[24] Furthermore, in the case of CO_2 separation utilizing pure 1-butyl-3-methylimidazolium nitrate ($BMIM^+NO_3^-$), the ideal CO_2/N_2 selectivity and CO_2 permeance were 4.7 and 5.2 GPU, respectively.[25]

To enhance the CO_2 separation performance of neat ILs, our group investigated selective CO_2 separation utilizing ILs with lithium tetrafluoroborate ($LiBF_4$).[26] It was established that the facilitated transport membrane consisting of lithium tetrafluoroborate as a CO_2 carrier and $BMIM^+BF_4^-$ exhibits an ideal selectivity of 8.40 for CO_2/N_2 with a CO_2 permeance of 13.36 GPU.[26] Lee *et al.* reported that a 1-methyl-3-octylimidazolium tetrafluoroborate ($MOIM^+BF_4^-$)/positively polarized Cu nanoparticle membrane shows CO_2/N_2 and CO_2/CH_4 selectivities of 25.2 and 24.3, respectively, with a CO_2 permeance of 24.2 GPU.[27] In addition, our group reported that $BMIM^+NO_3^-$/Cu nanoparticle membranes demonstrate a CO_2 permeance of 9.8 GPU with an ideal selectivity of 12.25 for CO_2/N_2 and CO_2/CH_4.[25] These results indicated that Cu NPs could be an excellent carrier for CO_2 separation in ILs.

Department of Chemistry, Sangmyung University, Seoul 110-743, Republic of Korea. E-mail: swkang@smu.ac.kr; Fax: +82 2 2287 5362; Tel: +82 2 2287 5362

Very recently, our group reported that metal oxide nanoparticles could be utilized for a CO_2 separation membrane. For example, an $MOIM^+BF_4^-$/AgO composite membrane showed a high ideal selectivity of 23.4 for CO_2/N_2, with a CO_2 permeance of 18.7 GPU; on the other hand, the neat $MOIM^+BF_4^-$ membrane showed a selectivity of 15.9, with a CO_2 permeance of 12.7 GPU.[28] Furthermore, when AgO particles were added to $BMIM^+BF_4^-$, a CO_2/N_2 selectivity of 28.2 and CO_2 permeance of 14.1 GPU were reported.[29] These results indicated that the dissociated AgO nanoparticles have strong affinity for CO_2 due to the oxide layer.[29]

In this study, in order to clarify the effect of the metal oxide in ILs, experiments were conducted with other oxides. Copper(II) oxide was selected because its properties are similar to those of silver oxide. For the $BMIM^+BF_4^-$/CuO composite membrane, the dissociated CuO particles were expected to enhance the solubility of the CO_2 molecules due to the nano-oxide particle layer. Moreover, when CuO was incorporated into $BMIM^+BF_4^-$, the free ions could also enhance the solubility of CO_2 molecules since the quadrupole moment of CO_2 was relatively higher than N_2, resulting in the increased separation performance.

II. Experimental

2.1 Materials

$BMIM^+BF_4^-$ was purchased from Merck KGaA (Darmstadt, Germany). CuO was purchased from Sigma-Aldrich Chemical Co. Ethyl alcohol (>94.0% purity) was purchased from Daejung Chemicals & Metals. All chemicals were used as received.

2.2 Characterization

A sonifier (Branson 450, Branson Ultrasonics Corporation, Danbury CT, USA) with a standard tip was used. Scanning electron microscopy (SEM) images were obtained using a JEOL JSM-5600LV system. Transmission electron microscopy (TEM) images were obtained using a JEM-2010 system operating at 200 kV. The weight loss was measured by thermogravimetric analysis (TGA, TGA Q50, TA Instrument) of the complex membrane in flowing N_2. FT-Raman measurements were performed for the $BMIM^+BF_4^-$/CuO solution at room temperature using a Horiba Jobin Yvon LabRam Aramis apparatus with a diode laser beam at an excitation wavelength of 785 nm.

2.3 Membrane preparation

The membranes were prepared utilizing $BMIM^+BF_4^-$, copper(II) oxide, and ethanol. First, copper(II) oxide was sonicated to disperse in ethanol for 5 min, and then, $BMIM^+BF_4^-$ was added into the mixture. The dispersion was heated at 85 °C for 24 h to evaporate ethanol. The final solution was coated onto a polysulfone support (Toray Chemical Korea Inc.) and then cast using an RK control coater (Model 202, Control Coater RK Print-Coat Instruments Ltd., UK). The best performance of $BMIM^+BF_4^-$/CuO was observed at a weight ratio of 1/0.007.

2.4 Gas separation performance

Gas flow rates were measured with a bubble flow meter at an upstream pressure of 2 kgf·cm^{-2} and atmospheric downstream pressure. The unit of gas permeance is GPU, with 1 GPU = 1×10^{-6} cm^3 (STP)/(cm^2 s cmHg). Selectivity was defined as ideal selectivity (CO_2 permeance/N_2 permeance).

III. Results and discussion

3.1 Transmission electron microscope (TEM) image of $BMIM^+BF_4^-$/CuO

TEM images were recorded to investigate the size and dispersity of the dissociated copper oxide particles in $BMIM^+BF_4^-$. As shown in Fig. 1, no significant copper(II) oxide agglomerates were present, and CuO particles were mostly observed as small nanoparticles with an average diameter of 10 nm. These results indicated that the dissociated CuO nanoparticles are advantageous for increasing the solubility of CO_2 molecules.

3.2 Separation performance

Fig. 2 presents the cross-section structures of the $BMIM^+BF_4^-$/CuO composite membrane. The utilized polysulfone support had a finger-like structure. The thickness of the coated selective layer was approximately 4.1 μm. Based on the SEM image, it was suggested that the selective layer was not penetrated into the polysulfone microporous support.

To investigate the effect of CuO concentration in the $BMIM^+BF_4^-$/CuO membrane on the CO_2 separation performance, the pure gas permeance of CO_2 and N_2 through the $BMIM^+BF_4^-$/CuO composite membrane was measured at increasing weight ratios of CuO, as shown in Fig. 3. As the CuO weight ratio increased, the CO_2 selectivity also sharply increased. As shown in Table 1, the highest CO_2 permeance (52.4 GPU) and CO_2/N_2 selectivity (21.0) were observed at a $BMIM^+BF_4^-$/CuO weight ratio of 1/0.007. At CuO weight ratios higher than 0.007, both CO_2 permeance and selectivity remained unchanged. However, above a CuO weight ratio of 0.04, the copper oxide was not well dispersed in $BMIM^+BF_4^-$, and therefore, significant copper oxide agglomerates were present. A previous study revealed that for neat $BMIM^+BF_4^-$, the CO_2 permeance and CO_2/N_2 selectivity were 17.0 GPU and 5.0, respectively, as shown Table 1.[24] On the other hand, when CuO was added to $BMIM^+BF_4^-$, the CO_2 permeance increased from 17 to 52.4 GPU and the CO_2/N_2 selectivity increased from 5.0 to

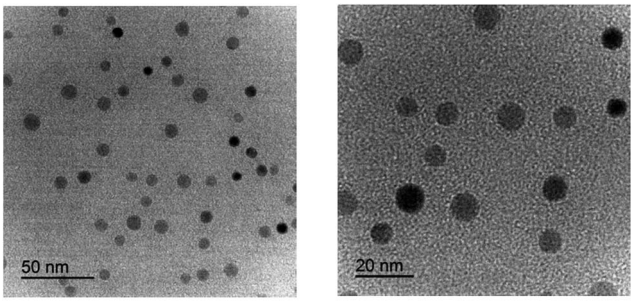

Fig. 1 (a) TEM image of the dissociated CuO nanoparticles in $BMIM^+BF_4^-$ and (b) enlarged image.

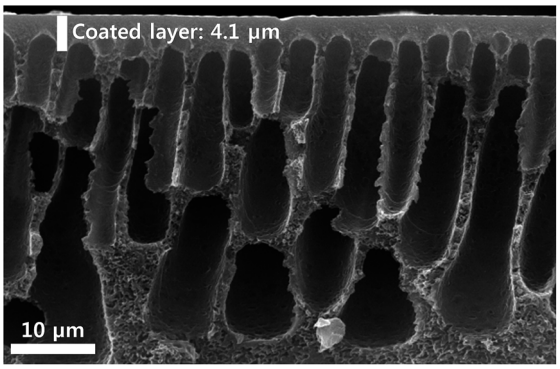

Fig. 2 SEM image of $BMIM^+BF_4^-$/CuO composite membrane.

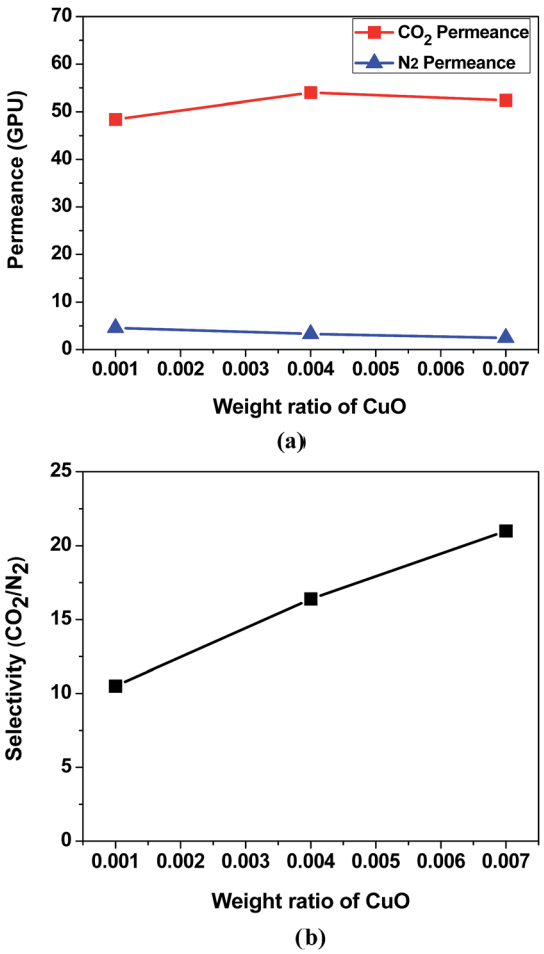

Fig. 3 Gas separation performance of $BMIM^+BF_4^-$/CuO composite membranes: (a) pure gas permeance and (b) ideal CO_2/N_2 selectivity.

21.0. Furthermore, it was confirmed that CO_2 permeance was much higher than the value reported in previous study consisting of BMIMBF4/AgO composite. (CO_2 permeance: 14.1 GPU)[29] These results were ascribed to two factors: (1) well-dispersed CuO nanoparticles, which could lead to enhanced CO_2 solubility due to the increased oxide layer and (2) abundant free ions in $BMIM^+BF_4^-$, enabling the enhanced CO_2 transport.

Table 1 Pure gas permeance and selectivity of neat $BMIM^+BF_4^-$ and $BMIM^+BF_4^-$/CuO membranes with a weight ratio of 1/0.007

	CO_2 permeance (GPU)	N_2 permeance (GPU)	CO_2/N_2 selectivity
Neat $BMIM^+BF_4^-$ (ref. 24)	17.0	3.4	5.0
$BMIM^+BF_4^-$/AgO[29]	14.1	0.5	28.2
$BMIM^+BF_4^-$/CuO	52.4	2.5	21.0

3.3 Thermogravimetric analysis

The thermal properties of the neat $BMIM^+BF_4^-$ and $BMIM^+BF_4^-$/CuO composite membranes were analyzed by TGA. Fig. 4 presents weight loss at temperatures from 350 to 500 °C. The major weight loss was ascribed to the structural decomposition of the IL $BMIM^+BF_4$. The $BMIM^+BF_4^-$/CuO composite showed slower decomposition with a smaller weight loss of 70.6% at 450 °C, as compared to that (53.2%) of neat $BMIM^+BF_4^-$ at the same temperature. If the agglomeration of CuO particles in $BMIM^+BF_4^-$ occurred, the decomposition temperature would remain constant. However, this result indicates that CuO particles were well dispersed in the IL $BMIM^+BF_4^-$, because of the coordinative interaction between the CuO surface and $BMIM^+BF_4^-$. Thus, the thermal stability of the $BMIM^+BF_4^-$/CuO composite membrane increased.

3.4 FT-Raman spectroscopy

Interactions between $BMIM^+BF_4^-$ and CuO in the $BMIM^+BF_4^-$/CuO composite membranes were investigated by FT-Raman spectroscopy. The Raman spectrum in the region of the BF_4^- stretching bands is shown in Fig. 5. Three different ionic species were observed in the FT-Raman spectra of the ILs: free ions, ion pairs, and ionic aggregates. The BF_4^- stretching bands at 765, 770, and 774 cm^{-1} were assigned to the free ions, ion pairs, and ion aggregates, respectively.[30] $BMIM^+$ forms ion aggregates and ion pairs with BF_4^- in $BMIM^+BF_4^-$ through hydrogen bonding.[24] A previous report showed that the Raman spectrum of neat $BMIM^+BF_4^-$ included signals attributed to ion

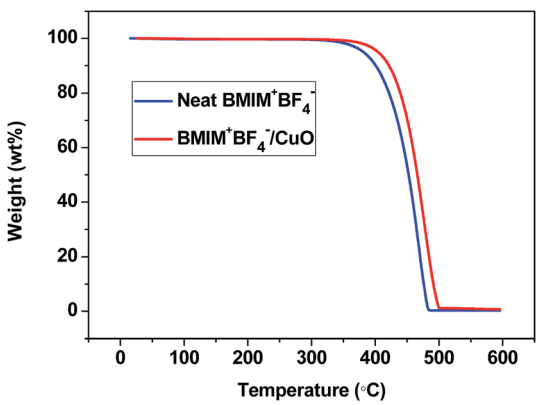

Fig. 4 TGA results for neat $BMIM^+BF_4^-$ (blue) and $BMIM^+BF_4^-$/CuO composite (red).

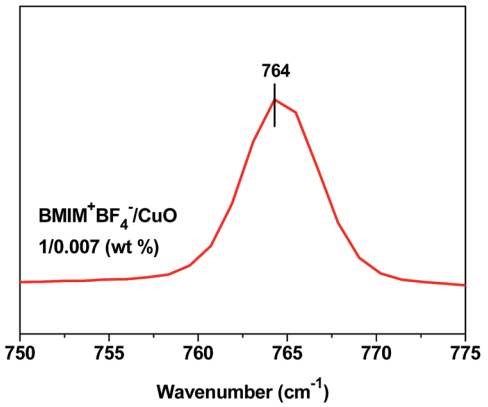

Fig. 5 FT-Raman spectrum of $BMIM^+BF_4^-$/CuO nanoparticles.

pairs and ion aggregates.[24] As the copper oxide is well dispersed in $BMIM^+BF_4^-$, free $BMIM^+$ and BF_4^- ions are observed. These results can be explained by the coordinative interaction between $BMIM^+BF_4^-$ and the surface of the CuO nanoparticles, which results in weakened interactions between $BMIM^+$ and BF_4^-. Therefore, CO_2 separation performance could be enhanced by the increase of solubility due to abundant free ions.

IV. Conclusions

We have successfully stabilized CuO nanoparticles by employing an ionic liquid $BMIM^+BF_4^-$. The coordinative interactions of the $BMIM^+BF_4^-$/CuO composite membrane were characterized by TEM, TGA, and FT-Raman analyses. The separation performance of the $BMIM^+BF_4^-$/CuO composite membrane was considerably enhanced compared to that of the neat $BMIM^+BF_4^-$. When CuO was incorporated into $BMIM^+BF_4^-$, the CO_2/N_2 selectivity increased to 21.0, with a CO_2 permeance of 52.4 GPU. These results were attributed to (1) the synergistic effect of well-dispersed CuO nanoparticles, which result in enhanced CO_2 solubility due to the increased surface of the oxide particle layer and (2) the abundant free ions in $BMIM^+BF_4^-$.

Acknowledgements

This work was supported by an Energy Efficiency & Resources grant from the Korea Institute of Energy Technology Evaluation and Planning (KETEP), funded by the Korean Government *via* the Ministry of Trade, Industry, and Energy (20122010100040). This work was also supported by the Basic Science Research Program (2017R1D1A1B03032583) through the National Research Foundation of Korea (NRF), and funded by the Ministry of Science, ICT, and Future Planning.

Notes and references

1 N. V. Blinova and F. Svec, *J. Mater. Chem. A*, 2014, **2**, 600–604.
2 N. Du, H. B. Park, M. M. Dal-Cin and M. D. Guiver, *Energy Environ. Sci.*, 2012, **5**, 7306–7322.
3 D. Aaron and C. Tsouris, *Sep. Sci. Technol.*, 2005, **40**, 321–348.
4 H. Q. Yang, Z. H. Xu, M. H. Fan, R. Gupta, R. B. Slimane, A. E. Bland and I. Wright, *J. Environ. Sci.*, 2008, **20**, 14–27.
5 J. Huang, J. Zou and W. S. Winston Ho, *Ind. Eng. Chem. Res.*, 2008, **47**, 1261–1267.
6 C. H. Yu, C. H. Huang and C. S. Tan, *Aerosol Air Qual. Res.*, 2012, **12**, 745–769.
7 O. Davidson and B. Metz, *International Panel on Climate Change*, 2005.
8 P. Jungho, K. Deukju and N. Sangyong, *Membr. J.*, 2015, **25**, 547–557.
9 P. arume and K. Sungjoong, *Membr. J.*, 2016, **26**, 126–134.
10 R. W. Baker and K. Lokhandwala, *Ind. Eng. Chem. Res.*, 2008, **47**, 2109–2121.
11 W. Yave, A. Car, J. Wind and K. V. Peinemann, *Nanotechnology*, 2010, **21**, 395301.
12 A. Meisen and X. Shuai, *Energy Convers. Manage.*, 1997, **38**, S37–S42.
13 W. J. Koros and R. Mahajan, *J. Membr. Sci.*, 2000, **175**, 181–196.
14 L. Deng, T. J. Kim and M. B. Hagg, *J. Membr. Sci.*, 2009, **340**, 154–163.
15 W. J. Ward and W. L. Robb, *Science*, 1957, **156**, 1481–1484.
16 R. Yegani, H. Hirozawa, M. Teramoto, H. Himei, O. Okada, T. Takigawa, N. Ohmura, N. Matsumiya and H. Matsuyama, *J. Membr. Sci.*, 2007, **291**, 157–164.
17 S. Kasahara, E. Kamio, T. Ishigami and H. Matsuyama, *Chem. Commun.*, 2012, **48**, 6903–6905.
18 S. U. Hong, J. H. Jin, J. Won and Y. S. Kang, *Adv. Mater.*, 2000, **12**, 968–971.
19 Y. Suzuki, H. Nishide and E. Tsuchida, *Macromol. Res.*, 2000, **33**, 2530–2534.
20 C. Yu, T. Zhu, X. Zhang and H. Liu, *Sci. Adv. Mater.*, 2015, **7**, 1213–1220.
21 J. Chang, G. H. Hong and S. W. Kang, *RSC Adv.*, 2015, **5**, 69698–69701.
22 P. T. Nguyen, B. A. Voss, E. F. Wiesenauer, D. L. Gin and R. D. Noble, *Ind. Eng. Chem. Res.*, 2013, **52**, 8812–8821.
23 K. E. Gutowski and E. J. Maginn, *J. Am. Chem. Soc.*, 2008, **130**, 14690–14704.
24 J. H. Lee, J. Hong, J. H. Kim, Y. S. Kang and S. W. Kang, *Chem. Commun.*, 2012, **48**, 5298–5300.
25 G. H. Hong, J. H. Oh, D. Ji and S. W. Kang, *Chem. Eng. J.*, 2014, **252**, 263–266.
26 Y. Choi, G. H. Hong and S. W. Kang, *J. Nanosci. Nanotechnol.*, 2016, **16**, 2832–2835.
27 J. H. Lee, J. Hong, J. H. Kim, D. Song, Y. S. Kang and S. W. Kang, *Chem. Eng. J.*, 2014, **235**, 252–256.
28 D. Ji and S. W. Kang, *Korean J. Chem. Eng.*, 2016, **33**(2), 666–668.
29 D. Ji, Y. S. Kang and S. W. Kang, *Sci. Rep.*, 2015, **5**, 16362.
30 S. W. Kang, D. H. Lee, J. H. Park, K. Char, J. H. Kim, J. Won and Y. S. Kang, *J. Membr. Sci.*, 2008, **322**, 281–285.